THE ASTROPHYSICAL JOURNAL, 352:149–158, 1990 March 20

AN ISOLATED, WELL-DEFINED INFRARED CIRRUS CLOUD

T. HERTER,[1,2] D. L. SHUPE,[2] AND D. F. CHERNOFF[3]
Center for Radiophysics and Space Research, Cornell University
Received 1989 June 30; accepted 1989 September 16

ABSTRACT

We present high spatial resolution (3.9) H I measurements of a high-latitude far-infrared cirrus cloud ($l = 9°$, $b = 51°$) obtained with the Arecibo 310 m telescope. The cloud, which is approximately 0.5×1.0 in size, is well isolated spatially and has a velocity well-separated from other H I clouds, providing an ideal laboratory for studying diffuse interstellar clouds. The H I column density is less than 2.1×10^{20} H-atom cm^{-2}. The internal H I velocity dispersion is 3–4 km s^{-1}. The systemic velocity ranges from -20 to -15 km s^{-1} (v_{LSR}), compared to the general Galactic background emission which is -4 km s^{-1} in this region of the sky. The $I_\nu(100)/N_H$ ratio is $0.52 \pm 0.05 \times 10^{-14}$ Jy sr^{-1} cm^2 and the $I_\nu(60)/I_\nu(100)$ ratio is 0.32 ± 0.03. Both values are comparable to previous measurements which averaged over larger angular sizes. Within the observational errors, the ratios are constant across the cloud.

The $I_\nu(100)/N_H$ and $I_\nu(60)/I_\nu(100)$ ratios are consistent with the Draine and Anderson model which includes a distribution of grain sizes down to 3 Å. The small grains undergo transient heating and affect the 60 μm far-infrared continuum emission. Current models, however, underpredict $I_\nu(12)/I_\nu(100)$ and $I_\nu(25)/I_\nu(100)$ by more than a factor of 2. We discuss some of the effects small grains will have on the thermal equilibrium of diffuse interstellar clouds. We also outline further work which will help elucidate the physics of this component of the interstellar medium.

Subject headings: high-latitude objects — interstellar: grains — interstellar: matter — nebulae: general — nebulae: internal motions

I. INTRODUCTION

In its 11 month survey, the *Infrared Astronomical Satellite* (*IRAS*; Neugebauer *et al.* 1984) scanned the large-scale structure of our Galaxy. Among its many unexpected discoveries was the "Galactic cirrus," patchy 60–100 μm emission, with a wispy, filamentary structure seen over the entire sky (Low *et al.* 1984). The cirrus emission originates in dust heated by absorbed Galactic radiation, which is then reradiated at longer wavelengths. Realistic models for the infrared emission require a range of dust particle sizes. The large grains, with radii greater than 100 Å, have nearly constant temperature (about 10–20 K) in which the time-averaged photon energy flux balances the grain's emissivity. The large grains provide the bulk of the emission at 60 and 100 μm. The small grains, on the other hand, undergo transient heating to temperatures in excess of 150 K, dominating the emission at 12 and 25 μm, and influencing it at 60 μm (Boulanger, Baud, and van Albada 1985; Draine and Anderson 1985; hereafter DA).

The cirrus emission is associated with both atomic and molecular phases of the interstellar medium (ISM). Boulanger, Baud, and van Albada (1985) showed that there exists a linear correlation between neutral hydrogen column densities, N_H, and 100 μm intensities, $I_\nu(100)$, in some high-latitude clouds. Terebey and Fich (1986) found a qualitatively similar, but quantitatively different correlation in two regions near $l = 125°$ and $l = 215°$ in the outer Galaxy, selected where the hydrogen is largely atomic, not molecular. Molecular emission is also associated with some high-latitude cirrus clouds (Weiland *et al.* 1986; see also de Vries, Heithausen, and Thaddeus 1987). CO emission occurs in the central portions of these 100 μm cirrus features indicating that the column densities are high enough to shield CO from destruction from the background interstellar radiation field. Recently, Boulanger and Pérault (1988) studied clouds in the solar neighborhood. They find a range in the correlation between N_H and $I_\nu(100)$ and attribute the variation to the intensity of the interstellar radiation field. Heiles, Reach, and Koo (1988; hereafter HRK), in a study of 26 isolated cirrus clouds, find a similar variation which they attribute to varying H_2 content and shock-processing of dust in the clouds. The intensity of the radiation field is closely connected with the abundance of molecules. Dust within the clouds can serve as a diagnostic of the radiation field since the nature of the illumination of the grains is crucial to their emission. In the high-latitude Galactic clouds, the primary heating source is thought to be the average Galactic background radiation (Spitzer 1978). However, closer to the Galactic plane, local heating sources can dominate the heating and can be intense enough to destroy small grains (Boulanger *et al.* 1988).

While cirrus emission is widespread, it can be studied only in the directions which are relatively unaffected by other confusing infrared sources along the line of sight, i.e., at high latitudes. ISM material above the Galactic plane is often associated with supernova-propelled shells or other large-scale stirring phenomena, such as stellar winds, moving clouds, and Galactic fountains. Study of the cirrus, in particular the velocity of the associated gas, its metal abundance, and the strength of the general Galactic radiation field, should help us eventually come to understand the grand mass motions of the ISM in our Galaxy.

[1] Guest Investigator, Infrared Processing and Analysis Center, which is operated by the California Institute of Technology for the National Aeronautics and Space Administration.

[2] Guest Observer at Arecibo Observatory. Arecibo Observatory is part of the National Astronomy and Ionosphere Center, which is operated by Cornell University for the National Science Foundation.

[3] Presidential Young Investigator.

The surveys of Boulanger, Baud, and van Albada (1985) and Terebey and Fich (1986) produced somewhat different values of the $I_\nu(100)$ to N_H ratio. These variations could be due to cloud-cloud differences in the dust-to-gas ratio, in the dust properties, or in the illuminating radiation field. HRK attribute the variation in part to molecule formation at low H I column densities. They find CO in clouds with column densities as low as $\sim 2.4 \times 10^{20}$ H-nuclei cm^{-2}. From the variation of the 60 to 100 μm flux ratio with velocity, HRK suggest that fast shocks destroy large grains or produce small grains. Both the Boulanger and Pérault (1988) and Terebey and Fich studies used the Weaver and Williams (1973) H I survey which has a spatial resolution of approximately 36′. The H I observations of HRK also have 36′ beam size. The 2′ resolution of the *IRAS* observations was degraded to match the H I data.

In this paper we focus on high-resolution observations of a single cloud which we show is isolated in space and in velocity from other H I clouds. The H I data obtained at Arecibo Observatory for this study have a spatial resolution comparable to that of *IRAS* at 100 μm. This allows a detailed examination of the gas and dust properties within a cloud. In § II we discuss the data set. In § III we analyze the $I_\nu(100)$ to N_H ratio and various infrared color ratios. In § IV we compare the observations to theoretical calculations of DA. We also discuss the physical location of the cloud and its relationship to the local ISM. Further studies which can aid in understanding the chemistry and thermal equilibrium of the cloud are briefly noted.

II. DATA AND OBSERVATIONS

The observations of the cirrus cloud presented in this paper are serendipitous in nature since they result from a search for swept dust from galaxies (Herter and Shupe 1989). We selected clusters of galaxies with minimal obscuration by Galactic cirrus emission on the basis of the *IRAS* skyflux plates. Several candidates were found including the cluster Abell 2040 which has a velocity of roughly 13,500 km s^{-1} (Dressler 1980). Infrared maps at the four *IRAS* bands (12, 25, 60, and 100 μm) were generated via the *IRAS* co-adding procedure with destriping on but flat-fielding off. Flat-fielding was performed afterward by selecting three reference fields around the 2° × 2° co-add field, fitting a plane to these three fields, and subtracting. Figure 1 shows the 100 μm contours from the *IRAS* co-added intensity map for the A2040 region. The bright infrared point source south of the center of the map is the galaxy ZW 1510+07. This galaxy is not located in the cluster. It has a recessional velocity of 3500 km s^{-1} and is an OH megamaser (Baan, Henkel, and Haschick 1987). We performed H I measurements to determine whether the dust emission is associated with ZW 1510+07 or is Galactic cirrus contamination. We found that the infrared emission correlates well with Galactic H I emission. In this paper we present a description of these H I observations and the infrared data. For more details of the extragalactic search see Herter and Shupe (1989).

Observations were made at the Arecibo Observatory located in Puerto Rico using the 21 cm flat feed. Since this feed reduces sidelobe response it is the best choice for mapping extended emission. The effective illumination area of the Arecibo dish with the flat feed is 210 m, resulting in a beam size of 3′.9. Data were taken using the 1024-channel correlator in frequency-switched mode with a 2.5 MHz bandwidth (0.51 km s^{-1} per channel). The plus signs and open circles in Figure 1 indicate the 92 positions at which spectra were obtained. The integration time at each position was 5 minutes. Since the region was accessible to Arecibo for only about 2 hr per day, the observations were spread over several days, and a complete mapping was not possible due to the limited time available.

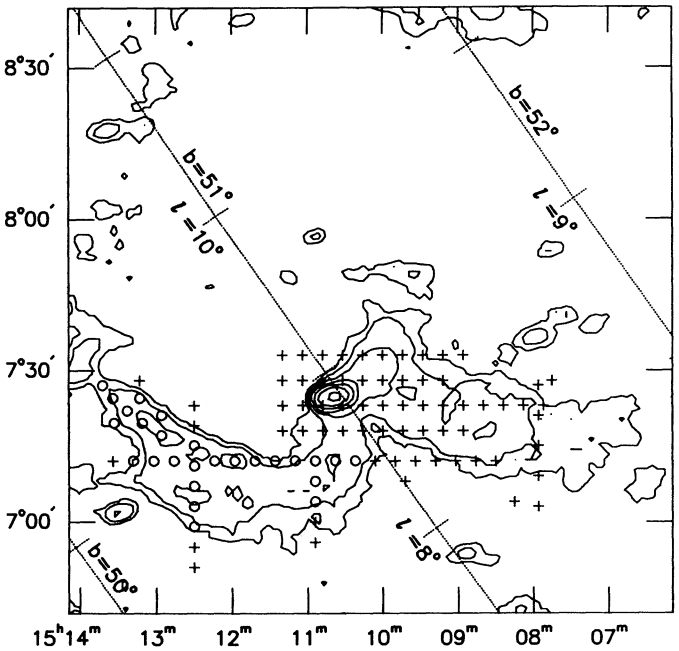

FIG. 1.—*IRAS* 100 μm intensity contour plot obtained by co-adding a 2° × 2° field. The contour levels are 0.25, 0.5, 1, 2, 4, 8, and 16 MJy sr^{-1}. The field has been flattened by subtracting a plane fit to three reference points outside the cloud. The bright point source is the OH megamaser galaxy, ZW 1510+07. The plus signs and open circles represent positions at which H I spectra were obtained. The open circles indicate the spatial positions within the eastern portion of the cirrus cloud with well-determined H I and 100 μm fluxes. Galactic latitude and longitude are also indicated.

All data were obtained by frequency switching rather than spatial switching because of the extended nature of the Galactic H I emission. Initially we used a frequency switch of 500 km s^{-1} with center frequencies of 0 and ±250 km s^{-1} to search for any high-velocity gas. No H I emission was found outside a velocity range of ±50 km s^{-1}. Thereafter, observations were made with a frequency switch of 250 km s^{-1} so that the H I line appeared in both the on and off frequency positions. The source was divided by the off-source (frequency) position to correct for responsivity variations across the bandpass. Since Galactic H I is so strong and the off position contains the line, simply dividing would have resulted in a substantial error in the H I flux. The parts of the on and off frequency-switched spectra outside the line (the opposite halves of the spectra in our case) were combined to give a background for division. The spectra in both positions were then combined by shifting, inverting, and averaging. The GALPAC routines in the spectral reduction package ANALYZ were used to apply a single Hanning smoothing to the data and subtract off the baselines. A correction was applied for the change in gain with zenith angle of the telescope for extended sources (Bania 1986). This was checked by observing the same position at several zenith angles. The accuracy of the calibration and the reproducibility of the pointing were investigated by observing the same spatial position on several nights. These checks indicate an error of less than 10%.

Figure 2 shows a sample reduced and calibrated spectrum.

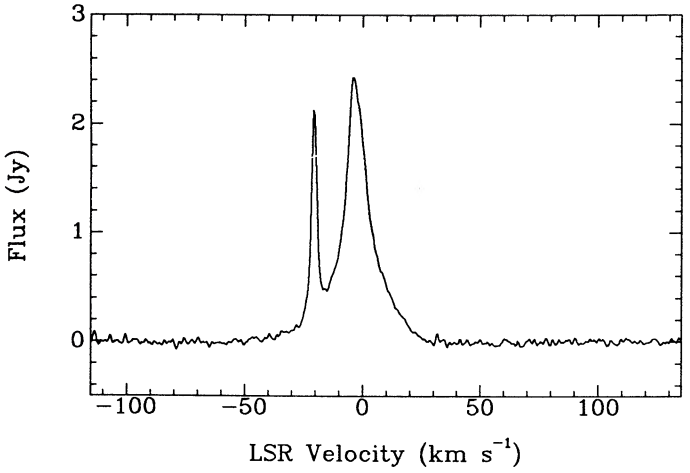

FIG. 2.—H I spectrum obtained at (α, δ) = ($15^h13^m23^s$, 7°22′00″), with Arecibo telescope using frequency switching in 5 minutes of integration. The spectral resolution of the observations is 0.51 km s^{-1} which has been smoothed to approximately 0.75 km s^{-1} using a Hanning smoothing function. The strong emission at −4 km s^{-1} is the general Galactic background emission (GGB), while the bright wing at −20 km s^{-1} is due to emission from the infrared cirrus cloud. The H I beam size is 3′.9.

The rms noise is approximately 25–30 mJy for all spectra. For conversion to antenna temperature, the nominal gain of the 21 cm flat feed is 6 K Jy^{-1} (Giovanelli and Haynes 1983; Bania 1986). The flux calibration was checked by observing calibrators at the beginning and end of each 2 hr observing run. In addition, our measured intensity for the general background H I emission in the direction of the cloud agrees well with that of the Heiles and Habing (1974) survey. The H I spectra at all 92 positions are presented in Figure 3. The velocity range plotted for each spectrum is −45 to +35 km s^{-1}. Contour maps of position versus velocity for four representative slices through the cloud are displayed in Figure 4.

III. RESULTS

a) Cloud Distinction

Figure 2 shows two distinct H I components, a 5–7 km s^{-1} wide line with broad wings centered at −4 km s^{-1} and a narrower feature at about −20 km s^{-1}. Many of the H I spectra show this behavior (Fig. 3). Comparison of Figures 1 and 3 shows that the narrow component is associated with the infrared cirrus cloud. Positions off the cloud show the broad feature but lack the narrow one. We associate the broad line with the general Galactic background H I emission (GGB). Choosing ZW 1510+07 (ZW), the bright infrared point source near the center, to be our reference point, the infrared emission region east of ZW shows a strong correlation between the H I brightness and the 100 μm intensity. The extended infrared emission west of ZW possibly manifests itself as H I emission wings on either side of the GGB profile or an increase in the peak intensity of the GGB depending on the spatial position observed. The separation of the GGB and the cirrus cloud is not distinct for most of the region west of ZW. Thus, we restrict our discussions to the eastern portions of the H I/IR filament.

The well-defined velocity and lack of confusing nearby infrared and H I emission make the eastern filament an excellent region to study the chemistry, composition, and thermal equilibrium of cirrus clouds. Figure 4 illustrates the H I velocity separation of the eastern portion of the cloud from the GGB. Velocity gradients are seen in the east-west scan (Fig. 4*a*), while north-south scans show roughly a constant velocity across the cloud (Fig. 4*c*). The exact geometry is ambiguous but the velocity gradient indicates a relatively short dispersal time for the cloud (see § IV*b*).

To measure the H I intensity over the cloud, an average GGB profile was subtracted from each of the original spectra. Due to slight changes in intensity, line width, and spectral positions even for regions in which only GGB was present, the subtraction process did not completely remove the GGB. Some of the residuals at the GGB center frequency could be due to shifts in the reference frequency supplied to the autocorrelator. The internal reference source used for these observations is accurate to ±0.25 km s^{-1}. In any case, the eastern portion of the cirrus cloud is well defined in velocity and of sufficient strength to make extraction of accurate H I column densities possible. The errors in N_H are dominated by these GGB removal problems and were estimated by comparing the values obtained from this subtraction process to a slightly different scheme in which the peak of the average profile was scaled to match the peak in each spectrum. The adopted value for the uncertainty is 0.08 × 10^{20} H-atom cm^{-2}.

b) H I−I_ν(100) Correlation

Given the small transition probability for $F = 1$ to 0, 21 cm H I line ($A = 2.84 \times 10^{-15}$ s^{-1}), the level populations will nor-

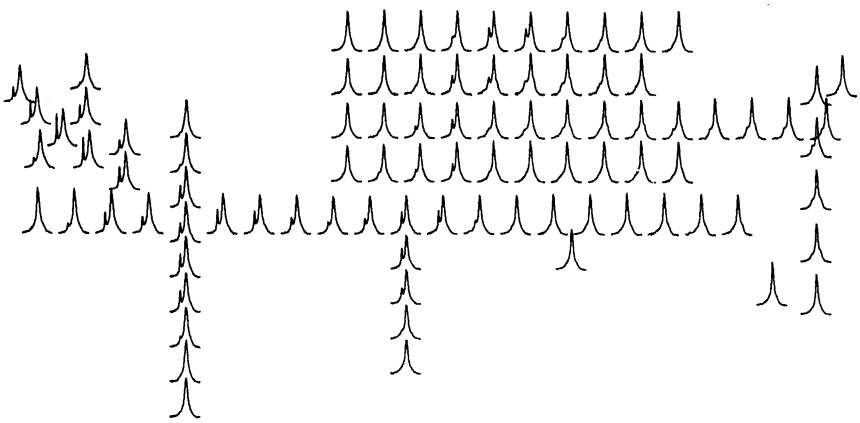

FIG. 3.—H I spectra obtained at the spatial positions indicated in Fig. 1. The arrangement of the spectra on the plot corresponds to their spatial position on the infrared map. All spectra are plotted on the same velocity and flux scale.

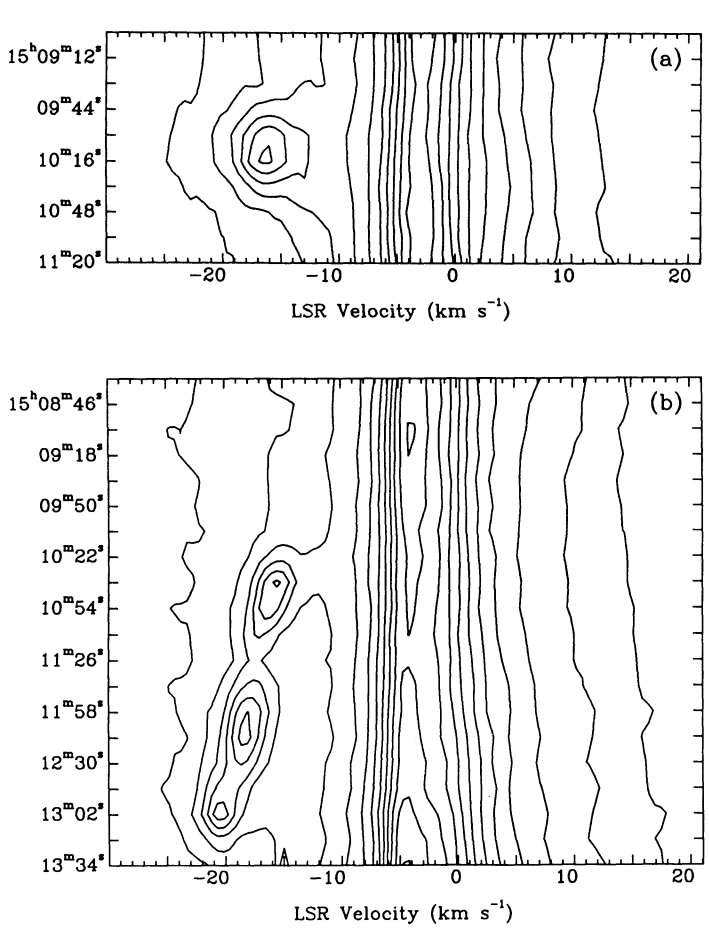

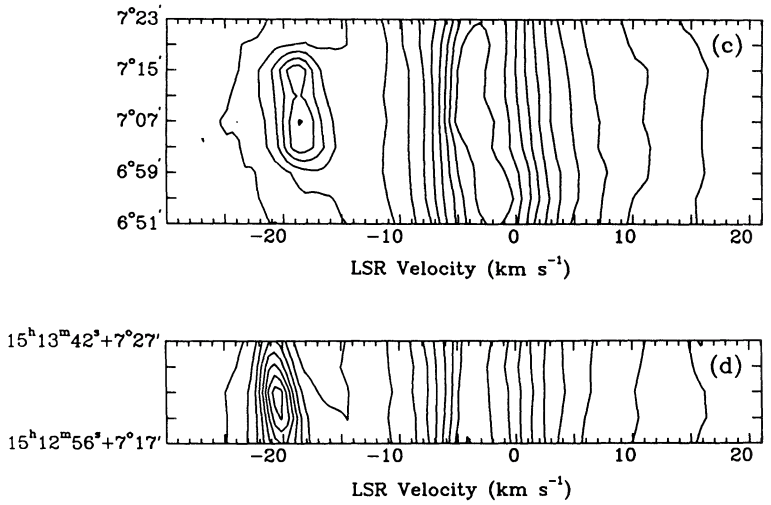

FIG. 4.—Velocity-spatial position contour plots at (*a*) $\delta = 7°33'$, (*b*) $\delta = 7°12'$, (*c*) $\alpha = 15^h12^m30^s$, and (*d*) the northeastern region of the cloud. Contour levels are in multiples of 250 mJy starting at 250 mJy. Each tick-mark on the vertical axes corresponds to an H I spectrum.

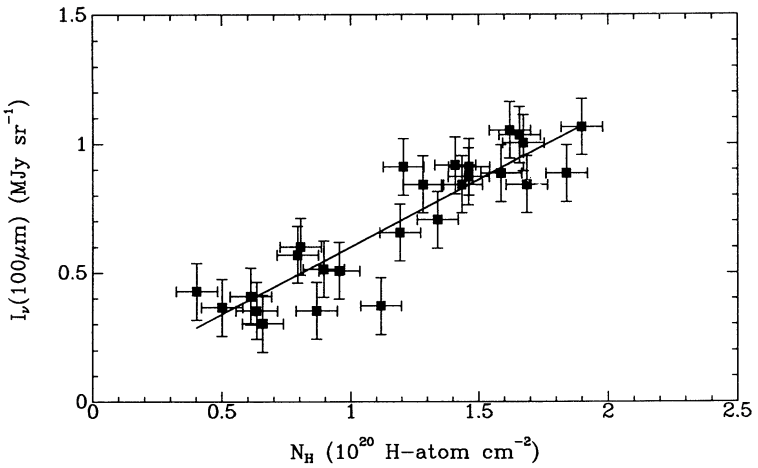

FIG. 5.—Plot of $I_\nu(100)$ vs. N_H for data from the eastern portion of the cirrus cloud. Only points from the eastern portion of the cloud with good signal-to-noise ratios and located far from the galaxy ZW 1510+07 have been included. Spatial positions which have been included in the plot are indicated by circles in Fig. 1. The solid line is a linear fit to the data which gives $I_\nu(100)/N_H = 0.52 \pm 0.05 \times 10^{-14}$ Jy sr^{-1} cm^2.

mally be in thermal equilibrium with the gas. If the emission is optically thin the H I column density is computed as

$$N_H = \frac{4.45 \times 10^{17}}{\theta_b{}^2(')} \left(\frac{S}{\text{mJy km s}^{-1}}\right) \text{cm}^{-2}, \quad (1)$$

where θ_b is the beam diameter and S is the integrated line profile,

$$S = \int S_v \, dv \, . \quad (2)$$

As a check on our assumption that the H I emission is optically thin, we compute the optical depth at line center. Over most of the cloud the H I line width is 3–4 km s^{-1}. This sets an upper limit to the gas temperature of 400–720 K. The H I optical depth at line center is

$$\tau_c = 0.0456 \left(\frac{\Delta v}{3 \text{ km s}^{-1}}\right)^{-1} \left(\frac{T}{400 \text{ K}}\right)^{-1} \left(\frac{N_H}{10^{20} \text{ cm}^{-2}}\right), \quad (3)$$

where Δv is the line width and T is the gas temperature. In the eastern portion of the cloud $N_H < 2.1 \times 10^{20}$ cm^{-2} for all positions, giving $\tau_c = 0.10$ for $T = 400$ K. For $\tau_c \geq 1$, the gas temperature must be below 40 K. Thus, the assumption of optically thin emission is justified.

In order to compare the H I and *IRAS* data, we extracted fluxes from the 60 and 100 μm co-added fields by summing pixel values in $\sim 4'$ diameter circles placed at the same positions as the H I data. Errors in these values were estimated by examining the fluctuation in similarly derived fluxes at several positions off the cloud. The data set includes only those points in the eastern region with a signal-to-noise ratio greater than 4 σ in both H I and $I_\nu(100)$, and well-separated from ZW 1510+07; these positions are marked by circles in Figure 1. We have plotted $I_\nu(100)$ versus N_H for these points in Figure 5. A linear fit to the data gives $I_\nu(100)/N_H = 0.52 \pm 0.05 \times 10^{-14}$ Jy sr^{-1} cm^2. A comparison with values found in other studies is given in Table 1. Our mean value for $I_\nu(100)/N_H$ is similar to that found by Terebey and Fich (1986) in a survey of infrared cirrus in the outer Galaxy but about a factor of 2 lower than that of Boulanger, Baud, and van Albada (1985). Our ratio is also somewhat higher than that determined by Boulanger and Pérault (1988) in an examination of the solar neighborhood.

The differences between Terebey and Fich (1986), Boulanger and Pérault (1988), and our result are significantly larger than the errors. The variations could be due to cloud-to-cloud differences in the dust-to-(H I) gas ratio or changes in the average dust temperature or both. Even within a single cloud there can be scatter in the $I_\nu(100)/N_H$ ratio for the same reasons. However, if the cloud is optically thin in the visual and there are no local heat sources, the dust is heated uniformly by the radiation field, which also prevents formation of H_2. For our

TABLE 1

IRAS INTENSITY AND H I DATA

Region	$I_\nu(100)/N_H$ (Jy sr^{-1}/H I atom cm^{-2})	$I_\nu(60)/I_\nu(100)$	Ref.
$l = 9°, b = 50°$	$5.2 \pm 0.5 \times 10^{-15}$	0.32 ± 0.03	1
$l = 125°, \lvert b \rvert < 10°$	$6.4 \pm 1.1 \times 10^{-15}$	0.21 ± 0.02	2
$l = 215°, \lvert b \rvert < 10°$	$4.2 \pm 0.8 \times 10^{-15}$	0.21 ± 0.02	2
$l \sim 115°, b \sim 72°$	$9.3 \pm 0.3 \times 10^{-15}$	...	3
$b > 50°$	$9.2 \pm 1.4 \times 10^{-15}$	0.29 ± 0.05	4
$b < -50°$	$7.9 \pm 0.6 \times 10^{-15}$	0.30 ± 0.08	4
$\lvert b \rvert > 10°$	$8.5 \pm 0.5 \times 10^{-15}$	0.21 ± 0.02	4
$150° < l < 170°, 15° < l < 30°$	$5.1 \pm 0.5 \times 10^{-15}$	0.21 ± 0.02	4

REFERENCES.—(1) This paper. (2) Terebey and Fich 1986. (3) Boulanger, Baud, and van Albada 1985, corrected for present *IRAS* calibration. (4) Boulanger and Pérault 1988.

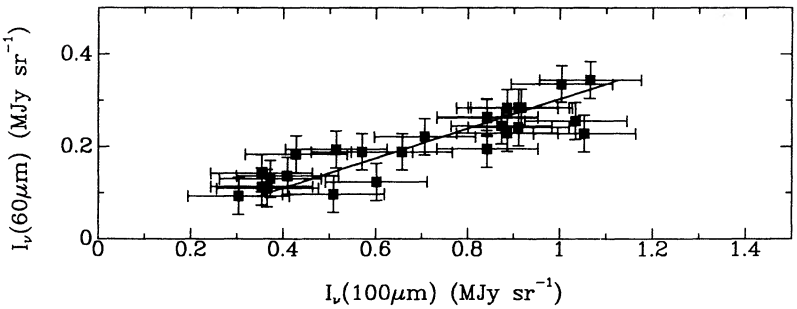

FIG. 6.—Infrared $I_\nu(60)$ vs. $I_\nu(100)$ for the same spatial positions used for Fig. 5. These positions are indicated by the circles in Fig. 1. A linear fit, indicated by the solid line, yields $I_\nu(60)/I_\nu(100) = 0.32 \pm 0.03$.

cloud $N_H < 2.1 \times 10^{20}$ H-atom cm^{-2}. Assuming $A_v/N_H = 5.3 \times 10^{-22}$ mag cm^2 (Bohlin, Savage, and Drake 1978; Savage and Mathis 1979) then $A_v < 0.11$ for the cloud. Thus, variation of $I_\nu(100)/N_H$ within our cloud would be related to changes in dust abundance or dust properties. From our linear fit to $I_\nu(100)$–N_H data, we find $\chi^2/\mathrm{dof} = 1.08$ (dof ≡ degree of freedom) which indicates the variations we see across the cloud are consistent with the observational errors.

c) $I_\nu(60)/I_\nu(100)$

Figure 6 displays $I_\nu(60)$ versus $I_\nu(100)$ for the eastern filament. The mean $I_\nu(60)/I_\nu(100)$ ratio is 0.32 ± 0.03. This ratio is significantly higher than that found by Terebey and Fich (1986, see Table 1); however, it agrees with some of the regions surveyed by Boulanger and Pérault (1988) and the isolated clouds studied by HRK. Assuming an emissivity law which varies as λ^0 or λ^{-1}, the dust color temperature is 36.2 ± 1.4 or 30.2 ± 1.0, respectively. Since the *IRAS* fluxes are computed assuming $f_\nu \propto \nu^{-1}$, a correction which depends on the intrinsic energy distribution must be applied to give the actual $I_\nu(60)/I_\nu(100)$ ratio. Using Table B.1 of Lonsdale *et al.* (1985) which converts between catalog fluxes and source temperature for different emissivity laws, our mean $I_\nu(60)I_\nu(100)$ ratio gives $T = 36$ and 30 K for emissivity laws which vary as λ^0 or λ^{-1}, respectively. These results are identical to our earlier calculations and can be attributed to the fact that at these dust temperatures the flux corrections to the 60 and 100 μm bands are similar. Uncertainties in the long wave cutoff of the *IRAS* 100 μm band can result "in significant errors in the flux densities for objects colder than 30 K" (*IRAS Explanatory Supplement* 1985). We have not attempted to account for this uncertainty in the quoted errors; however, as with our earlier determination of $I_\nu(100)/N_H$, effects due to systematic offsets in the *IRAS* intensities are irrelevant for calculating $dI_\nu(60)/dI_\nu(100)$, the slope in Figure 6. Using our estimated error, we find $\chi^2/\mathrm{dof} = 1.2$ for the fit. Our data are consistent with no variation in the $I_\nu(60)/I_\nu(100)$ color across the cloud.

d) $I_\nu(60)/I_\nu(100)$ – H I Correlation

We have also examined $I_\nu(60)/I_\nu(100)$ color ratio as a function of N_H. No color changes are present with increasing N_H column density. The mean $I_\nu(60)/I_\nu(100)$ ratio is again 0.32 and the slope is -0.01 ± 0.04. The $\chi^2/\mathrm{dof} = 0.50$. The data are consistent with a fixed $I_\nu(60)/I_\nu(100)$ ratio independent of N_H, although the small value of χ^2/dof probably indicates we have overestimated the errors somewhat. The 60 and 100 μm flux uncertainties were added in quadrature, which is correct if they are uncorrelated. In spite of the variation in N_H, the uniformity in $I_\nu(60)/I_\nu(100)$ strengthens our assertions that the cloud is optically thin and the dust temperature is uniform.

e) Integrated IRAS Flux Ratios

To obtain reliable values for $I_\nu(12)/I_\nu(100)$ and $I_\nu(25)/I_\nu(100)$, it was necessary to integrate over the entire eastern portion of the cloud. One-dimensional spectra were produced from 9° × 9° co-added fields by summing pixels along a diagonal strip of approximately the same length and orientation as the eastern arm. The strip was moved along the declination direction of the fields to generate each spectrum. Parabolic baselines were fitted to regions north and south of the cloud and subtracted from the spectra to remove the zodiacal background. The resulting spectra are shown in Figure 7. To obtain error estimates for the integrated fluxes, we compared the rms fluctuations of empty regions near the cloud to errors obtained by fitting two Gaussian components to the integrated profiles. The latter method yielded somewhat larger and, we believe, more realistic errors for the integrated fluxes, and were used to compute the uncertainties in the flux ratios. The adopted values of these ratios are listed in Table 2. The value of $I_\nu(60)/I_\nu(100)$ agrees within errors with the ratio derived from fitting a line to the $I_\nu(60)$ to $I_\nu(100)$ data (§ IIIc). While $I_\nu(60)/I_\nu(100)$ is the same as that found by Boulanger, Baud, and van Albada (1985), $I_\nu(12)/I_\nu(100)$ and $I_\nu(25)/I_\nu(100)$ are factors of 2.9 and 2.7 times higher for the present cloud than to the one they examined. This may indicate a greater population of small grains in the cloud we are studying. These ratios fall within the range of values observed by HRK.

IV. DISCUSSION

a) Cloud Location

At this point we pause to consider the physical location of the serendipitously discovered cloud within the Galaxy. Later

TABLE 2

IRAS COLORS[a]

λ (μm)	$I_\nu(\lambda)/I_\nu(100)$
12.....	0.087 ± 0.012
25.....	0.11 ± 0.02
60.....	0.28 ± 0.03

[a] Ratios obtained by integrating over the eastern portion of the cirrus cloud.

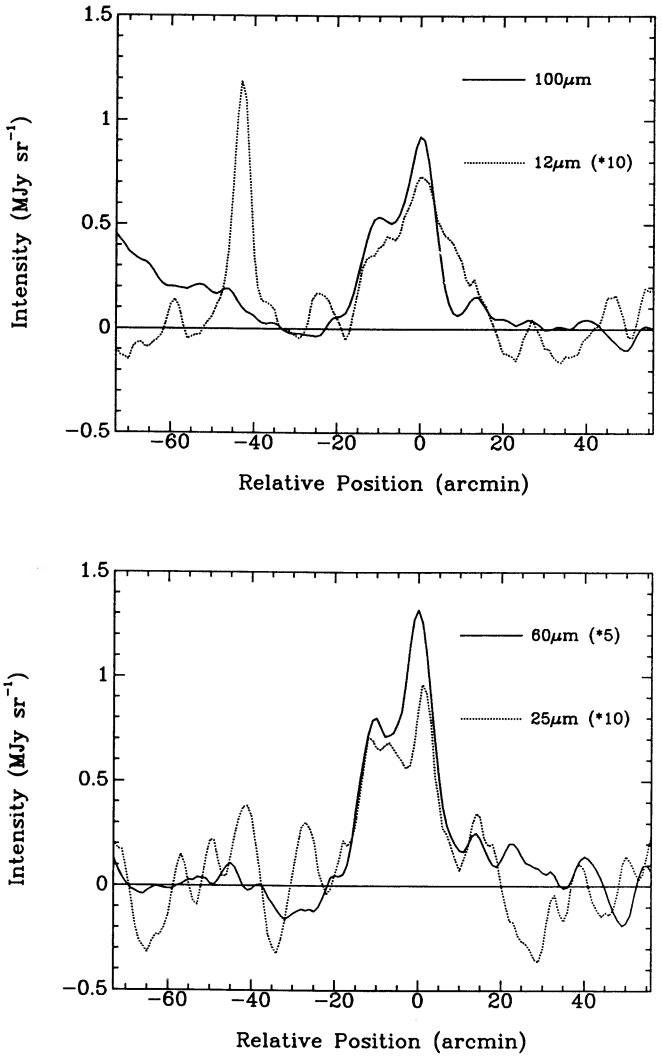

FIG. 7.—One-dimensional spectra obtained by integrating *IRAS* 9° × 9° co-added fields over the eastern arm of the cloud. The horizontal axis corresponds to the declination direction, and the tick-marks are spaced by 5′. To produce each point in the spectra, pixel values were summed along a diagonal strip of approximately the same orientation and length as the eastern arm (position angle equals 63°.4). The sharp peak to the left of the cloud is the 12 μm profile of a weak point source.

we study the relationship of the dust and gas emissions and the internal kinematics. In principle a distance estimate to the cloud can be obtained via a spectroscopic parallax technique. Measurements of stars which lie on either side of the cloud can be used to bracket its distance. Far stars will show absorption lines associated with the velocity of the cloud while those on the near side would not. This technique has been used by Hobbs, Blitz, and Magnani (1986) and Hobbs *et al.* (1988) to obtain distance estimates of high-latitude molecular clouds. Unfortunately the small size of the cloud in the current study makes this technique difficult to apply. In lieu of direct information on the cloud distance, we make some arguments on the possible location of the cloud based on kinematic arguments and current knowledge of the local ISM.

Figure 1 illustrates that the cloud is present in a rectangle (l, b) = ([8–10]°, [50–52]°) and Figures 4*a–d* shows that the typical velocity range is $V_{LSR} = -14$ to -22 km s^{-1}. Several lines of reasoning support the hypothesis that the cloud is an

TABLE 3

LOCAL INTERSTELLAR CLOUDS[a]

Area	Cloud	l	b	Dist. (pc)	$E(b-y)$
3C 317.....	1	13°	51°	70–101	0.030
	2	9	52	~165	0.052
	3	7.5	51	143–255	0.016
	4	5	50	~202	0.040
	5	9	48.5	81–100	0.038

[a] Data on clouds in the direction of (l, b) = (9°, 51°) from Knude (1979).

isolated, local object. The crudest estimates follow directly from V_{LSR}. The cloud's velocity components in the plane are not dominated by the Galaxy's rotation which produces recession in the first quadrant. This gives only a weak constraint since l is small. The magnitude of V_{LSR}, if a similar component is directed out of the plane, yields a 170 pc scale height in the Bahcall (1984) model of the Galactic potential perpendicular to the disk and implies that the cloud does not oscillate through the plane with large amplitude.

Observations of the local interstellar medium place some constraints on the cloud's location. Based on color excess measurements in A and F stars, Knude (1979) detected five clouds in an area centered around the extragalactic source 3C 317 which are near our cloud (see Table 3). Knude's cloud sizes are determined to about 1° so that his clouds 2 and/or 3 may coincide with ours. Using Knude's conversion, $N_H = 7.5 \times 10^{21}\ E(b-y)$ atom cm^{-2}, the column densities are 3.9×10^{20} atoms cm^{-2} and 1.2×10^{20} atoms cm^{-2}, respectively. These are consistent in order of magnitude with the observed H I column densities. The inferred distances are less than 165 pc and 143–255 pc, respectively. An examination of the 100 μm *IRAS* sky plate did not show any obvious emission at the locations of any of Knude's clouds 1 to 5, save at our cloud; however, large-scale (> 2′) diffuse infrared emission features are difficult to identify.

The Perry and Johnson (1982) photometric study of interstellar reddening includes three stars (see Table 4) within the area of interest (the Galactic latitude is uncertain by ±0°.4). They are at distances 101, 96, and 76 pc and have $N_H \leq 7.5 \times 10^{19}$ atoms cm^{-2}. [The relatively small extinction at high latitude is not unexpected; the maps of Perry and Johnson show that the mean color excess $E(b-y) \leq 0.070$ over all regions (15° × 15°) with $b > 30°$.] These strongly suggest that the cloud is a *localized* entity, constrained in angular size by the three slightly reddened stars around it to $\Delta\theta \lesssim 1°$. This is consistent with both the H I and infrared data which indicate the localized nature of the cloud. Further study is necessary to determine if it matches one of Knude's clouds (no. 2 or 3).

TABLE 4

STELLAR REDDENING[a]

Star	l	b	Dist. (pc)	$E(b-y)$
HD 134793.....	10°.2	52°.0	101	0.000
HD 135203.....	9.4	51.1	196	0.010
HD 135927.....	10.4	50.3	76	0.010

[a] Data on stars in the direction of (l, b) = (9°, 51°) from Perry and Johnson 1979.

How close might the detected cloud be? The very local ISM appears to have a uniform motion, as deduced by optical interstellar absorption lines (Crutcher 1982) and well fitted by $V_0 = -28$ km s^{-1} (heliocentric reference system) from the direction $(l_0, b_0) = (25°, 10°)$. The radial heliocentric velocity observed along the line of sight (l, b) is

$$\frac{V}{V_0} = \sin b \sin b_0 + \cos b \cos b_0 \cos (l - l_0) .$$

The motion of the ISM in the direction $b = 51°$, $l = 9°$ gives the heliocentric velocity $V = -20.5$ km s^{-1}, which is to be contrasted with the cloud's *observed* heliocentric motion of $V = -30$ to -34 km s^{-1}. Thus the cloud is approaching the Sun more quickly than the very local ISM, and it suggests that the cloud lies at least 10–20 pc away. Bochkarev's (1987) model and Bzowski's (1988) reanalysis of the absorption line data estimate the region to be of this size. Their physical model is a cloudlet accelerated by the stellar wind of the Sco-Cen association. The H I column density is a maximum 10^{20} atoms cm^{-2} in the direction of the Sancisi-Van Woerden filament ($l = 350°$, $b = 20°$). The presently studied H I cloud lies along the extension on the sky of the Sancisi-Van Woerden filament and within the Tinberg polarization patch which traces the angular outline of the cloudlet in Bochkarev's (1987) model. The close angular proximity, similar column density, and upper limit to the distance discussed below (about 40 pc), all suggest that there is a connection between the very local material and the cloud.

An upper limit to the distance to the cloud may be estimated if we adopt the Weaver (1979) proposal that the stellar winds from the Sco-Cen association cleared a large cavity within which a supernova subsequently exploded (see Fig. 8). Weaver estimates the center of loop I, the supernova shell, to be $(l_1, b_1) = (336°, 24°)$ with less than 2° uncertainties. The angular radius of loop I is $\Delta\theta = 55.^{\circ}5$. Simple geometry implies that the line of sight to the cloud makes an angle $\gamma_{12} = 32°$ with the center of loop I. *Thus the line of sight to the cloud pierces the SNR.* The line-of-sight distance d to cross the supernova shell is

$$d = \frac{h}{\cos b_1} [\cos \gamma_{12} \pm (\sin^2 \Delta\theta - \sin^2 \gamma_{12})^{1/2}] ,$$

where h is the distance *in the plane* to the center of loop I, estimated to be about 170 pc. This yields $d = 42$ pc for the near intersection and $d = 270$ pc for the far side. Distances between the two extremes are probably excluded. A cloud lying *inside* the supernova remnant would be quickly ionized and evaporated. If it passed through the shock front, it would be shredded and given large velocity. It may be that the cloud lies on the far side of loop I; however, it has an *inward* radial velocity toward the Sco-Cen center which has no obvious explanation. Thus we are left with the possibility that the cloud is closer to us than about 42 pc. In the Weaver scenario it is part of the original stellar wind or that wind's interaction with the H I cavity. This cloud is quite possibly the "smoking gun" of the Weaver scenario and deserves further study.

b) *Gas Properties*

If we adopt as a distance estimate of the cloud $d = 40$ pc, then the angular size of $\frac{1}{2}°$ implies a characteristic size $l \approx 0.35$ pc $d_{40\mathrm{pc}}$, where $d_{40\mathrm{pc}} = d/(40$ pc). The cloud density is roughly $n(\mathrm{H}) = N_{\mathrm{H}}/l \approx 80$–$200$ cm^{-3} $d_{40\mathrm{pc}}^{-1}$ for the range of detected H I column density. The cloud mass is approximately $M = 0.4$–1.0 $M_\odot$ $d_{40\mathrm{pc}}{}^2$. If the cloud were in thermal pressure balance with the general ISM, then $nT = 3600$ K cm^{-3}, so $T \approx 19$–45 K $d_{40\mathrm{pc}}$. However, neither the inferred thermal velocity dispersion ($\langle v^2 \rangle^{1/2} = (kT/\mu)^{1/2} \approx 0.36$–$0.56$ km/5 $d_{40\mathrm{pc}}{}^{1/2}$) nor the inferred gravitational velocity dispersion ($\langle v^2 \rangle^{1/2} \approx (GM/l)^{1/2} \approx 0.07$–$0.11$ km s^{-1} $d_{40\mathrm{pc}}{}^{1/2}$) is large enough to give the observed line-of-sight velocity dispersion of a few km s^{-1}. In addition, there is a resolved velocity gradient across the cloud of about 4 km s^{-1} ($dv/dx \approx 11$ km s^{-1} pc^{-1} $d_{40\mathrm{pc}}{}^{-1}$) which implies that the cloud will disperse in a time $t_d \approx l/v \approx 8.8 \times 10^4$ yr $d_{40\mathrm{pc}}$. The relatively short dispersal time and the large overpressure ($\rho \langle v^2 \rangle / k = 1.9$–$4.6 \times 10^5$ deg K cm^{-3} $d_{40\mathrm{pc}}{}^{-1}$ where we have used the observed velocity dispersion) suggests that the cloud was recently shocked. HRK have claimed large values of $I_\nu(60)/I_\nu(100)$ are indicative of shocks and shock processing of grains. (They derive an empirical relationship between larger $|v_{\mathrm{LSR}}|$ and larger $I_\nu(60)/I_\nu(100)$.) Our single cloud has a higher ratio of $I_\nu(60)/I_\nu(100)$ than all but five of the 26 HRK clouds. This is consistent with the suggestion that it too has been shocked, although its $|v_{\mathrm{LSR}}|$ is small. The distorted shape of the cloud on the sky supports such an interaction and it may be consistent with the "smoking gun" scenario discussed above. The true physical temperature is almost certainly greater than the thermal pressure balance argument suggests and we discuss some estimates in § V.

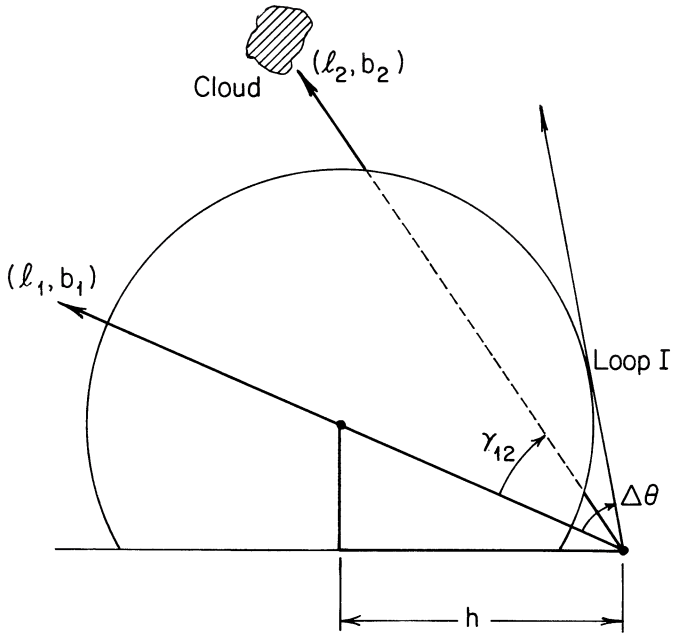

FIG. 8.—Geometry of the SNR remnant loop I and the cloud. See text for details.

c) *Dust Properties*

DA have modeled the expected $I_\nu(60)/I_\nu(100)$ ratios versus $I_\nu(100)/N_{\mathrm{H}}$ for different grain models and for various intensities of the interstellar radiation field. They included temperature fluctuations in the dust grains in their calculations and predict *IRAS* intensities by integrating over the spectral response of the *IRAS* bands. The dust distribution is assumed to follow a modified form of the distribution proposed by Mathis, Rumpl, and Nordsieck (1977, hereafter MRN) to account for interstellar extinction. Taking dn_i to be the number density of grains

of type i in the interval $[a, a + da]$, the DA model is

$$dn_i = A_i n_H a^{-3.5} da \quad (a_b < a < a_{max})$$
$$= A_i n_H a_b^{0.5} a^{-4.0} da \quad (a_{min} < a < a_b), \quad (4)$$

where n_H is the hydrogen number density, a_{min} is the minimum grain size, a_{max} is the maximum grain size, a_b is the radius which marks the transition between the MRN distribution and the region of enhancement of small grains. The MRN determination requires $a_{min} \leq 0.01$ μm but otherwise does not constrain the lower cutoff. If MRN is extended to $a_{min} = 3$ Å only 1% of the carbon atoms are incorporated into grains of size $3 < a < 6$ Å. By contrast, Léger and Puget (1984) find that $\sim 6\%$ of the carbon atoms are contained in these small grains, on the basis of the strength of the previously "unidentified" infrared features. DA correct for the deficiency in small grains predicted by the MRN power law by introducing the distribution given above. Selecting $a_b = 100$ Å enhances the small grain population to agree closely with the Lĕger and Puget (1984) mass estimates.

Figure 9 displays the different DA models. As indicated in the plot $a_{min} = 3$ Å, while a_b varies between a_{min} and 100 Å. $a_{max} = 0.25$ μm except for the model which displays the largest $I_\nu(60)/I_\nu(100)$ ratio which has $a_{max} = 0.1$ μm. The ambient ultraviolet interstellar radiation field is taken to be either 0.5, 1, or 3 times that in the solar neighborhood. DA used this graph to discuss the properties of cirrus clouds measured by Low *et al.* (1984). We have indicated the location of the present cloud on the diagram. Its location shows that within the intrinsic error bars of our determination, the cloud falls near the modified MRN (DA's best guess) power law.

DA predict $I_\nu(12)/I_\nu(100) = 0.022$ and $I_\nu(25)/I_\nu(100) = 0.058$ for their enhanced small grain population case. These values are about 2–4 times lower than the measured radios for our cloud (Table 2). DA note such a discrepancy between their $I_\nu(12)/I_\nu(100)$ estimates and at least one dark cloud, Lynds 255. They point out that some aspects of the physics of small grains may not be treated properly or that additional heating mechanisms for the small grains might exist. In any case, the discrepancy is intriguing and deserves further observational and theoretical attention. For instance, PAHs which have a different spectral signature than the silicates and graphite grains used by DA (Léger and Puget 1984) may better account for the observed ratios.

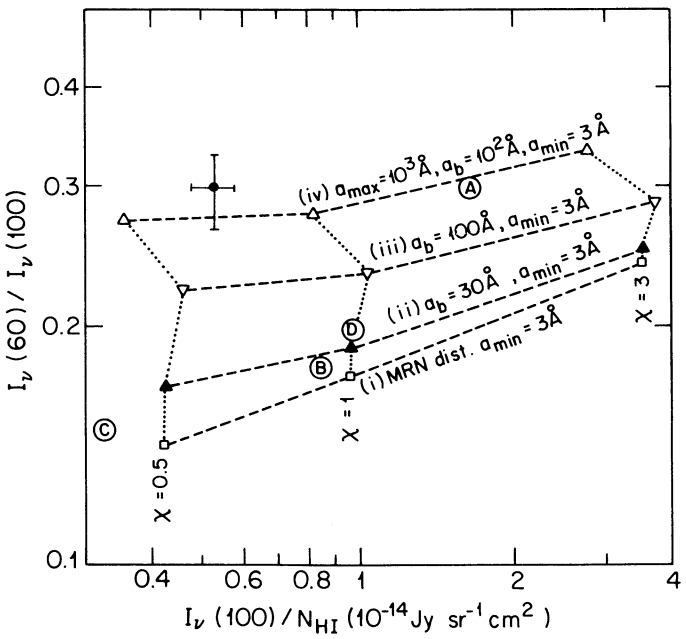

FIG. 9.—Predicted *IRAS* flux ratio $I_\nu(60)/I_\nu(100)$ vs. $I_\nu(100)/N_H$ from Draine and Anderson (1985) for various grain models and for intensities of ($\chi =$) 0.5, 1, 3 times the local radiation field (see text). Points label A, B, C, and D are data on cirrus clouds from Low *et al.* (1984) as plotted by Draine and Anderson. Data from the eastern filament of the cirrus studied here is indicated by the cross. The average value of the $I_\nu(60)/I_\nu(100)$ from Tables 1 and 2 has been used.

V. GENERAL CONSIDERATIONS

In principle, the cloud provides an excellent environment to study the basic processes of diffuse clouds, unhindered by the complications of radiative transfer. In particular, the relationship of photoelectron heating of the gas and fine structure cooling may be explored. The measured column density of H I is too small to allow the formation of large amounts of H_2. Observationally, the threshold for significant molecule formation is $E(B-V) \approx 0.08$, or $N(H\ I + H_2) \approx 5 \times 10^{20}$ atoms cm^{-2} (Savage *et al.* 1977). Theoretical models of diffuse clouds (van Dishoeck and Black 1986) show that molecule formation depends upon the UV radiation field, and the gas density and temperature. Van Dishoeck and Black (1986) constructed detailed models to fit observations along the line of sight to ξ Per. Model B of that paper (Table 4 in their paper), while not directly applicable to our cloud, does provide plausible estimates of the gas properties. The central density of this hydrostatically supported model is $n_H = 325$ cm^{-3} and the central temperature is $T_0 = 30$ K. However, we will not be concerned with the inner regions, but rather the outer parts. Model B has a total $A_v = 1.02$, so the total column density of material is larger than found in our cloud. If we treat the results as indicative, we can use the outer 10^{18} cm of the model (corresponding to $N_H \approx 1.6 \times 10^{20}$ cm^{-2}). The external radiation field of the models is twice the average UV field, so for our application, the outer layers receive *approximately* the average UV radiation field. The surface number density of H is about 100 cm^{-3} and the surface temperature is about 170 K. At a distance of 10^{18} cm from the outer edge, the H density is 90 cm^{-3}, the H_2 density is 30 cm^{-3}, and the temperature is 140 K. The small changes make it plausible that self-gravity is not an important effect in the outer parts of the model. The cloud ion fraction is dominated by C^+ with density of 0.04–0.06 cm^{-3}. In this model the neutral carbon abundance is always less than 10^{-4} cm^{-3}.

We now roughly calculate the rate of grain photoelectric heating and fine structure cooling implied for the physical parameters outlined above. For Draine's standard models (1978) the rate of photoelectric heating in the above conditions is approximately $\Gamma_d \approx 8.0 \times 10^{-27} - 2.5 \times 10^{-26}$ ergs per nuclei s^{-1} (Fig. 5*a* of Draine 1978). Heating by photoionization of atomic carbon, or gas grain collisions in this environment is unimportant (using the estimates in Black 1987). Cooling is predominantly by excitation of C II fine structure transitions. The cooling rate by electron plus hydrogen excitation of the C II at 150 K is $\Lambda_{C\,II} = n(C^+)[n(e)3.5 \times 10^{-21} + n(H)1.0 \times 10^{-23}]$ ergs cm^{-3} s^{-1} (Dalgarno and McCray 1972) and is dominated by hydrogen collisions. For our cloud the total cooling in C II is approximately $\Lambda_{C\,II} \approx 4.4 \times 10^{-23}$ ergs cm^{-3} s^{-1}, compared with the total photoelectric heating

rate $\Gamma_d \approx 2.5 \times 10^{-24}$ ergs cm^{-3} s^{-1} (taking the larger values in the range). The models of van Dishoeck and Black (1986) do not satisfy energy balance in the outer regions (as they note). It is an outstanding problem to resolve this discrepancy (Black 1987). Additional heating by large molecules (e.g., PAHs) may contribute to the effective heating of the gas (Lepp and Dalgarno 1988; d'Hendecourt and Léger 1987). Alternately, small grains may be crucial. For a review of heating of interstellar gas by dust see Hollenbach (1989).

Based on the above cooling rate, we estimate a C^+ line flux from the northern ridge of the cloud of approximately 5×10^{-20} W cm^{-2} in a 1′ beam. The isolated and well-defined boundary to part of the cloud make measurements of the C^+ 157 μm line from the Kuiper Airborne Observatory (KAO) possible. This predicted flux should be within reach of current KAO sensitivities (cf. Strutzki *et al.* 1988). Measuring the C II emission should pin down half of the solution since it represents the main cooling mechanism. Indirectly this allows a determination of the net photoelectric heating. The efficiency of grain photoelectric heating is especially uncertain in the regime of grain sizes of order the electron mean free path (50 Å, Draine 1978). As we have shown above, the DA theoretical results already constrain the properties of the grains to some extent, and it becomes of interest to try and understand whether the same model which gives the appropriate 60 μm (relative to 100 μm) infrared fluxes can also accommodate the 12 and 25 μm fluxes as well as the required photoelectric heating.

VI. CONCLUSIONS

We have performed high spatial resolution (3.9) H I measurements of a high-latitude far-infrared cirrus cloud ($l = 9°$, $b = 51°$) obtained with the Arecibo 310 m telescope. The cloud is well-defined in velocity and occupies an angular size of 0.5 × 1.0 on the sky. The internal H I velocity dispersion is 3–4 km s^{-1}. The systemic velocity ranges from −15 to −20 km s^{-1} (v_{LSR}), compared to the general Galactic background emission which is −4 km s^{-1}. The H I column density is less than 2.1×10^{20} H-atom cm^{-2}. The $I_\nu(100)/N_H$ ratio is $0.52 \pm 0.05 \times 10^{-14}$ Jy sr^{-1} cm^2 and the $I_\nu(60)/I_\nu(100)$ ratio is 0.32 ± 0.03. These values fall within the range of surveys by Terebey and Fich (1986), Boulanger and Pérault (1988), and Heiles, Reach, and Koo (1988).

Comparison of the observed $I_\nu(100)/N_H$ and $I_\nu(60)/I_\nu(100)$ ratios for the cloud with the calculations of Draine and Anderson (1985) shows that a small grain population exists in the cloud. The transient heating of the grains affects the 60 μm far-infrared continuum emission causing the far-infrared colors to be different from that expected for larger nonfluctuating grains. The $I_\nu(12)/I_\nu(100)$ and $I_\nu(25)/I_\nu(100)$ ratios for the cloud are significantly greater than the largest ratios predicted by Draine and Anderson. We obtain $I_\nu(12)/I_\nu(100) = 0.087 \pm 0.012$ and $I_\nu(25)/I_\nu(100) = 0.11 \pm 0.02$ whereas Draine and Anderson calculate 0.022 and 0.058 respectively for these ratios in their enhanced small grain population case. Further studies involving H I absorption line measurements, VLA mapping, Zeeman-splitting studies, optical absorption line observations, and C^+ cooling measurements will help understand the physics of the cloud (and others).

We have benefited from discussions with Leo Blitz, Bruce Draine, Bruce Elmegreen, Dave Hollenbach, Shri Kulkarni, and Chris McKee. We thank the staff of IPAC for their excellent support and in particular Nick Gautier and Walter Rice. We thank George Helou for discussions concerning methods for deriving dust temperatures and their accuracy. Willem Baan, Tony Phillips, and John Salzer were instrumental in helping us schedule our observations and reduce the data at Arecibo. Martha Haynes lent her expertise to ensure that the H I data were calibrated properly. We would particularly like to thank Riccardo Giovanelli for personally checking the calibration by independently reducing some of our H I data. The Arecibo telescope operators ensured that the correlator and telescope were set up and working properly. T. H. acknowledges partial support for this work by NASA grant JPL 23085. D. L. S. gratefully acknowledges support through an NSF Graduate Fellowship during part of this work. D. F. C. acknowledges support of NSF grant AST-86-57467.

REFERENCES

Baan, W. A., Henkel, C., and Haschick, A. D. 1987, *Ap. J.*, **320**, 154.
Bahcall, J. N. 1984, *Ap. J.*, **287**, 926.
Bania, T. M. 1986, Performance of the 1407 MHz Flat Feed Radiometer System, internal Arecibo Observatory memorandum.
Black, J. H. 1987, in *Interstellar Processes*, ed. D. J. Hollenbach and H. A. Thronson, Jr. (Boston: Reidel).
Bochkarev, N. G. 1987, *Ap. Space Sci.*, **138**, 229.
Bohlin, R. C., Savage, B. D., and Drake, J. F. 1978, *Ap. J.*, **224**, 132.
Boulanger, F., Baud, B., and van Albada, G. D. 1985, *Astr. Ap.*, **144**, L9.
Boulanger, F., Beichman, C., Desert, F. X., Helou, G., Pérault, M., and Ryter, C. 1988, *Ap. J.*, **332**, 329.
Boulanger, F., and Pérault, M. 1988, *Ap. J.*, **330**, 964.
Bzowski, M. 1988, *Acta Astr.*, **38**, 443.
Crutcher, R. M. 1982, *Ap. J.*, **254**, 82.
Dalgarno, A., and McCray, R. A. 1972, *Ann. Rev. Astr. Ap.*, **10**, 375.
d'Hendecourt, L. B., and Léger, A. 1987, *Astr. Ap.*, **180**, L9.
de Vries, H. W., Heithausen, A., and Thaddeus, P. 1987, *Ap. J.*, **319**, 723.
Draine, B. T. 1978, *Ap. J. Suppl.*, **36**, 595.
Draine, B. T., and Anderson, N. 1985, *Ap. J.*, **292**, 494 (DA).
Dressler, A. 1980, *Ap. J. Suppl.*, **42**, 565.
Giovanelli, R., and Haynes, M. P. 1983, Spectral Line Manual, internal Arecibo Observatory report.
Heiles, C., and Habing, H. J. 1974, *Astr. Ap. Suppl.*, **14**, 1.
Heiles, C., Reach, W. T., and Koo, B-C 1988, *Ap. J.*, **332**, 313 (HRK).
Herter, T., and Shupe, D. L. 1989, in preparation.
Hobbs, L. M., Blitz, L., and Magnani, L. 1986, *Ap. J. (Letters)*, **306**, L109.
Hobbs, L. M., Blitz, L., Penprase, B. E., Magnani, L., and Welty, D. E. 1988, *Ap. J.*, **327**, 356.
Hollenbach, D. J. 1989, in *IAU Symposium 135, Interstellar Dust*, ed. A. G. G. M. Tielens and L. Allamandola (Dordrecht: Reidel).
IRAS Catalogs and Atlases, Explanatory Supplement 1985, ed. C. A. Beichman, G. Neugebauer, H. J. Habing, P. E. Clegg, and T. J. Chester (Washington, DC: US Government Printing Office).
Knude, J. 1979, *Astr. Ap. Suppl.*, **38**, 407.
Léger, A., and Puget, J. L. 1984, *Astr. Ap.*, **137**, L5.
Lepp, S., and Dalgarno, A. 1988, *Ap. J.*, **335**, 769.
Lonsdale, C. J. Helou, G., Good, J. C., and Rice, W. 1985, "Cataloged Galaxies and Quasars Observed in the IRAS Survey," JPL D-1932.
Low, F. J., *et al.* 1984, *Ap. J. (Letters)*, **278**, L19.
Mathis, J. S., Rumpl, W., and Nordseick, K. H. 1977, *Ap. J.*, **217**, 425 (MRN).
Neugebauer, G., *et al.* 1984, *Ap. J. (Letters)*, **278**, L1.
Paresce, F. 1984, *A.J.*, **89**, 1022.
Perry, C. L., and Johnston, L. 1982, *Ap. J. Suppl.*, **50**, 451.
Savage, B. D., Bohlin, R. C., Drake, J. F., and Budich, W. 1977, *Ap. J.*, **216**, 291.
Savage, B. D., and Mathis, J. S. 1979, *Ann. Rev. Astr. Ap.*, **17**, 73.
Spitzer, L., Jr. 1978, *Physical Processes in the Interstellar Medium* (New York: Wiley).
Strutzki, J., Stacey, G. J., Genzel, R., Harris, A. I., Jaffe, D. T., and Lugten, J. B. 1988, *Ap. J.*, **332**, 379.
Terebey, S., and Fich, M. 1986, *Ap. J. (Letters)*, **309**, L73.
van Dishoeck, E. F., and Black, J. H. 1986, *Ap. J. Suppl.*, **62**, 109.
Weaver, M. 1979, in *IAU Symposium 84, The Large Scale Characteristic of the Galaxy*, ed. W. B. Burton (Reidel: Dordrecht) p. 295.
Weaver, H., and Williams, D. R. 1973, *Astr. Ap. Suppl.*, **8**, 1.
Weiland, J. L., Blitz, L., Dwek, E., Hauser, M. G., Magnani, L., and Rickard, L. J. 1986, *Ap. J. (Letters)*, **306**, L101.

D. CHERNOFF, T. HERTER, and D. SHUPE: Center for Radiophysics and Space Research, Space Sciences Building, Ithaca, NY 14853